THE JOURNAL OF PHYSICAL CHEMISTRY C

Article

pubs.acs.org/JPCC

Slow Conductance Relaxation in Graphene–Ferroelectric Field-Effect Transistors

Steven P. Rogers,[†] Ruijuan Xu,[‡,§] Shishir Pandya,[‡,§] Lane W. Martin,[‡,§] and Moonsub Shim*[,†]

[†]Department of Materials Science and Engineering and Frederick Seitz Materials Research Laboratory, University of Illinois at Urbana–Champaign, Urbana, Illinois 61801, United States

[‡]Department of Materials Science and Engineering, University of California, Berkeley, California 94720, United States

[§]Materials Science Division, Lawrence Berkeley National Laboratory, Berkeley, California 94720, United States

Supporting Information

ABSTRACT: Tuning graphene conduction states with the remnant polarization of ferroelectric oxides holds much promise for a range of low-power transistor and memory applications. However, understanding how the ferroelectric polarization affects the electronic properties of graphene remains challenging because of a variety of intricate and dynamic screening processes that complicate the interaction. Here, we report on a range of slow electrical conductance relaxation behavior in graphene–ferroelectric field-effect transistors with the extreme case leading to the convergence of two polarization-induced states. Piezoresponse force microscopy through the graphene channel reveals that the ferroelectric polarization remains essentially unchanged during this conductance relaxation. When measured in vacuum, the conductance relaxation is significantly reduced, suggesting equilibration with adsorbates from the ambient atmosphere that can cause charge transfer to and from graphene to be the origin of the slow relaxation.

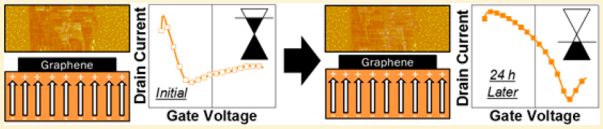

INTRODUCTION

Since its discovery[1,2] and the subsequent development of large-area growth techniques,[3−5] graphene has been considered for an extensive range of applications including chemical sensing,[6−9] flexible and transparent electrodes,[3,10,11] field-effect transistors (FETs),[12−14] and information storage devices.[15] This diversity of applications stems from its unique electronic structure in conjunction with robust mechanical and chemical properties all encompassed in an atomically thin material. With respect to FET and memory applications, interfacing graphene with ferroelectrics has been proposed to provide several benefits.[16−35] For example, ferroelectric gate oxides in graphene FETs can not only reduce the operating voltage as a result of the high dielectric constant[16] but also provide additional means of manipulating the Fermi level position with polarization direction.[22,26] For a structure consisting of graphene on top of a ferroelectric oxide substrate, UP polarization (i.e., polarization pointing toward the graphene) should, in theory, cause graphene to become more n-type, while DOWN polarization (i.e., polarization pointing away from the graphene) should induce more p-type behavior. These two states can be accessed simply with a small applied gate voltage (V_g) driving reversal of the polarization, opening the door to memory applications. Furthermore, patterning polarization domains with established methods allows spatially modulated doping of graphene.[26]

The coupling between the ferroelectric polarization direction and graphene Fermi level position is, however, complicated, as evidenced by several reports of the Dirac point (DP) shifting in both the expected and the unexpected directions in response to polarization switching in atmospheric conditions.[18−20,22,26] Here and throughout, DP shift refers to the shift in V_g at which the DP appears. Additionally, even when the DP shift is in the expected direction, the magnitude of the shift is significantly smaller than expected for a complete charge compensation of the ferroelectric polarization.[22] The polarization can be screened by charges from complicating factors at the interface such as adsorbed H_2O,[26] ferroelectric surface reconstructions,[26] charged defects, and impurities.[25] Further complications arise when one considers how the measurements are interpreted. One common approach to switch ferroelectric polarization in graphene–ferroelectric FETs is by sweeping V_g at a range above the coercive voltage. A shift in the conductance minimum corresponding to the DP can then be used to quantify changes in the Fermi level of the graphene. However, the underlying picture of the ferroelectric switching process, when analyzed in this manner, is complicated because of a wide range of factors, including adsorption–desorption of ambient molecules, substrate charging, and other factors that can all cause a shift in the V_g at which the DP appears and/or reduce the transconductance around the DP in graphene FETs. Incorporating an additional effect from polarization switching further complicates the interpretation of such measurements.

Additionally, there has been little direct experimental evidence for actual polarization switching under the graphene channel. Given that the intrinsic carrier concentration of graphene is an order of magnitude smaller than that required to completely compensate the remnant polarization of the ferroelectric oxide, the presence of a depolarization field and

Received: January 23, 2017
Revised: March 10, 2017
Published: March 10, 2017

DOI: 10.1021/acs.jpcc.7b00753
J. Phys. Chem. C 2017, 121, 7542−7548

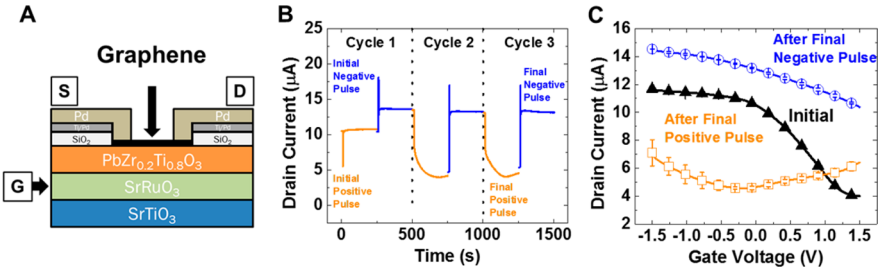

Figure 1. (A) Schematic device structure of the field-effect transistors studied. S, D, and G correspond to source, drain, and gate, respectively. (B) Drain current time trace during the initial poling process. Blue traces correspond to switching the polarization DOWN with −7 V, 1 s pulses, and orange traces correspond to switching the polarization UP with +7 V, 1 s pulses. (C) Gate voltage sweeps taken 250 s after the final switching operations compared to the initial transfer characteristics. Error bars represent the range of drain current values covered by the hysteresis between forward and reverse sweeps. Some data points have error bars smaller than the symbols.

thus the possible formation of antiparallel domains[36,37] cannot be ruled out. Knowing the polarization landscape is then critical to interpreting electrical measurements because nonuniform doping of the graphene channel can cause complications such as a change in V_g where the DP appears and reduced transconductance. Hence, separating out ferroelectric polarization effects from other extrinsic factors that influence graphene conductivity and doping level upon switching of polarization remains a critical task. Direct measurements of the polarization under the graphene has recently been performed using piezoresponse force microscopy (PFM).[24] However, the limited length scale that has been examined (~1 μm^2) makes it difficult to infer the polarization over the entire channel region of most graphene−ferroelectric FETs (which have areas of several to tens of square micrometers). PFM has also been used to examine polarization switching in $BaTiO_3$ using carbon nanotubes (CNTs).[38] In that study, the switched regions had widths much larger than those of CNTs and were imaged after the removal of CNTs, emphasizing the importance of paying careful attention to extrinsic effects including compensation of the ferroelectric polarization by adsorbates from the ambient surrounding. Here, we study graphene FETs with $PbZr_{0.2}Ti_{0.8}O_3$ (PZT) as the gate oxide and observe a slow conductance relaxation of varying degree over several hours. In some cases, this slow relaxation can lead to a complete convergence of the two states initially set by polarization switching. On the basis of PFM measurements over the entire graphene channel area, we conclude that this slow equilibration process is not caused by the relaxation of the ferroelectric polarization. Furthermore, we observe a significant suppression of this relaxation phenomenon in vacuum, indicating equilibration between the ambient molecules and graphene is responsible for the observed effect.

METHODS

Graphene was grown using an established chemical vapor deposition method on Cu foil (99.999% Puratronic, Alfa Aesar).[39] Raman spectra of the graphene transferred to Si/SiO_2 do not exhibit detectable D-band, as shown in the Supporting Information (Figure S1). The one-touch transfer method described in ref 22 was used to transfer the graphene onto a 150 nm PZT film grown by pulsed laser deposition on a $SrTiO_3$ (001) substrate with a 20 nm $SrRuO_3$ serving as the bottom electrode. Before graphene was transferred to the PZT substrate, the surface was characterized with PFM. The surface scans revealed a smooth sample surface (~150 pm roughness) as well as a uniform polarization orientation, as shown in the topography and phase images in panels A and B of Figure S2, respectively. Additional measurements revealed that the as-grown polarization state of the PZT was in the UP direction, as indicated in Figure S2D. Before graphene transfer, the PZT film and substrate were annealed at 300 °C for 30 min under 500 sccm O_2 flow to remove residual surface contaminants. Upon transfer of the graphene, electrical contacts were defined using standard photolithography techniques. The device structure has been previously reported[22] and is schematically shown in Figure 1A. First, 100 nm SiO_2 islands were deposited by electron-beam evaporation, which was followed by 3 nm/25 nm Ti/Pd layers. An additional 25 nm Pd layer was deposited to contact the graphene. We found the SiO_2 islands necessary to reduce leakage current between the Pd and $SrRuO_3$ contacts as previously reported.[22] A channel width of 5 μm and length of 3 μm were defined by standard photolithography using AZ 5214E photoresist and O_2 plasma etching. Atomic force microscopy (AFM) topography measurements revealed the presence of a residue layer after device fabrication. This thin layer was removed by scanning the channel with an AFM tip operating in the contact mode with a 100 nN scanning force. Representative channel topography images as well as V_g sweeps before and after AFM cleaning are shown in the Supporting Information (Figure S3). Initial poling of the devices was carried out by cycling 7 V, 1 s pulses of alternating polarity for a total of 3−5 cycles. The time trace of this initial poling process is shown in Figure 1B for a device that required three sequential cycles of switching. It was found that this initial poling procedure led to more reproducible results and maximized the graphene DP shift with ferroelectric polarization switching. Electrical measurements were performed using an Agilent 4156C semiconductor parameter analyzer. Gate voltage pulses were applied using a BK Precision 4052 arbitrary waveform generator. PFM measurements were performed using an Asylum Cypher AFM running in dual AC resonance tracking (DART) mode[40] with a scanning force of 10 nN and tip voltage <1 V. Vacuum measurements were carried out in a home-built vacuum probe station operating at a pressure of 10^{-6} Torr.

RESULTS AND DISCUSSION

The graphene FETs studied herein are schematically shown in Figure 1A. Similar devices have been used to examine how the polarization of ferroelectric oxides can be switched by graphene and how it can, in turn, alter the carrier type and density in graphene. This coupling of the ferroelectric polarization direction with the graphene conduction is illustrated in Figure 1B which plots the time trace of the graphene drain current (I_d)

DOI: 10.1021/acs.jpcc.7b00753
J. Phys. Chem. C 2017, 121, 7542−7548

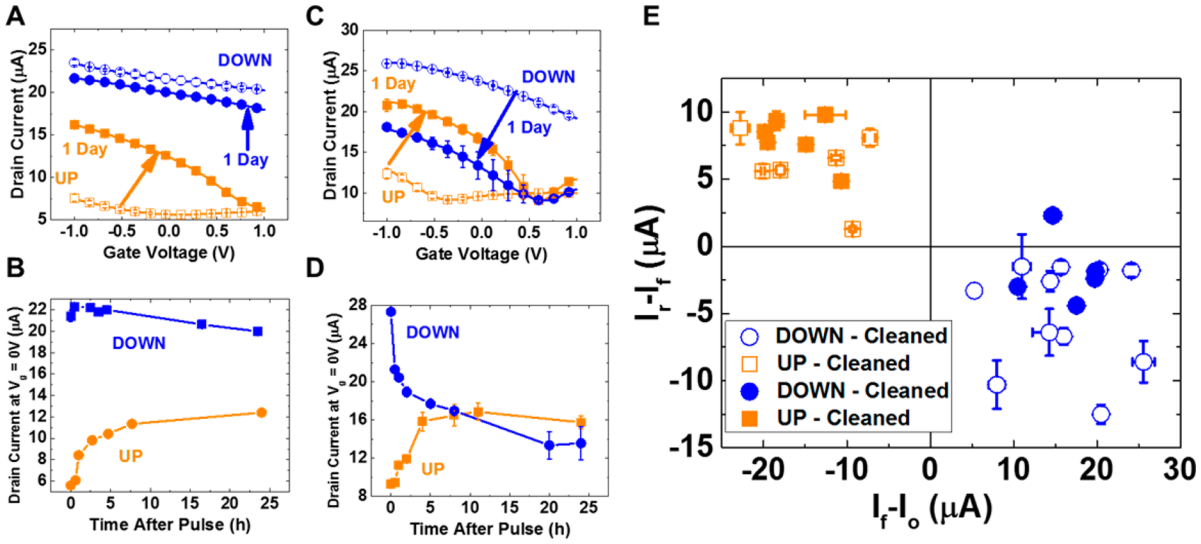

Figure 2. (A) Transfer characteristics of a typical graphene−ferroelectric FET showing asymmetric relaxation for the UP and DOWN states. (B) The drain current extracted at V_g = 0 V from I_d−V_g characteristics throughout the relaxation period plotted as a function of time for both the UP and DOWN states. Panels C and D show plots equivalent to those in panels A and B, respectively, for a device that exhibit the extreme case where both states relax to essentially the same conductance state. The error bars for panels A−D were estimated using the same method discussed in the caption for Figure 1C. (E) Amount of drain current relaxation over 24 h versus the initial change in current due to ferroelectric polarization switching for several different devices. Open symbols indicate devices that have undergone channel cleaning with the AFM tip, and solid symbols are those that have not. Error values along each axis were estimated as the square root of the sum of the squares of the two current error values, each of which were calculated as described in the caption for Figure 1C.

under a small bias of 50 mV during the initial cycling procedure (switching by sweeping V_g above the coercive voltage, verified by the DP shift and the peaks in the gate current at $V_g \sim \pm 2.5$ V, is shown in Figure S4). The orange time traces correspond to the graphene conductance state after the application of a square V_g pulse of 1 s duration and +7 V magnitude to the bottom contact, which should cause the polarization of the PZT to be poled UP. The blue time traces refer to the graphene conduction state after application of a square V_g pulse of 1 s duration and −7 V magnitude, switching the system to the DOWN polarization state. Within ∼250 s after applying each switching pulse, the device appears to have mostly equilibrated, indicating two stable states presumably induced by the two polarization states of the PZT. The expected changes in the I_d−V_g characteristics[22] are similar to what is shown in Figure 1C. Upon switching the polarization DOWN, the graphene becomes significantly more p-type, causing the DP to appear beyond the V_g window of the measurement. When the polarization is switched UP, the graphene becomes n-type with the DP appearing at $V_g \sim -0.5$ V, corresponding to an estimated electron density of 5.5×10^{12} cm^{-2}. Although the polarization of PZT can be switched with smaller and shorter V_g pulses in most devices, ±7 V pulses of 1 s duration were used here (unless noted otherwise) to ensure as complete of a switching of the polarization as possible.

An important aspect of graphene−ferroelectric FETs is the long-term stability of the ferroelectrically coupled graphene conduction states. Figure 1C suggests that the two polarization directions of the PZT lead to two stable p and n regimes as determined by the sign of the transconductance at V_g = 0 V. To explore the stability of these states, we monitored several devices over a longer time period, and Figure 2 shows the range of responses observed. Figure 2A,B provides an example when these two states are relatively stable. In Figure 2A, V_g dependence for both the UP and DOWN states immediately and 24 h after applying the switching pulses are shown. Multiple gate sweeps were performed over the course of this 24 h period, and I_d at V_g = 0 V is plotted as a function of time in Figure 2B. While there is only a small change for the DOWN polarization state, the UP state exhibits a significant relaxation within ∼7 h after switching. More extreme relaxation can be observed in some devices, as shown in Figure 2C, where the I_d−V_g characteristics converge with identical DP locations at ∼0.7 V. The corresponding time evolution of I_d at V_g = 0 V is shown in Figure 2D. That is, the two ferroelectric polarization-induced states of graphene eventually equilibrate to what appears to be the same state.

The slow relaxation behaviors for several devices are compared in Figure 2E by plotting the amount that I_d has relaxed over 24 h ($I_r - I_f$) versus the initial change in I_d upon polarization switching ($I_f - I_o$). Here, I_o is the initial current before switching and I_f and I_r are measured 250 s and 24 h after the switching pulse, respectively. These changes were calculated from I_d−V_g characteristics rather than from simple resistance measurements to take both the changes in carrier type and small hysteresis into consideration (Figure S5). When there was a change in carrier type, the additional change in the current that gets canceled out upon going through the minimum current (I_{min}) was taken into account (i.e., $I_f - I_o = -|I_f + I_o - 2I_{min}|$ and $I_r - I_f = +|I_r + I_f - 2I_{min}|$). Note that Figure 2E includes devices both with (open symbols) and without (filled symbols) cleaning off fabrication residues on the graphene channels with an AFM tip. Cleaning via AFM tip was necessary for the PFM measurements discussed below. Whether or not cleaned with an AFM tip, the range of the observed behavior is similar, suggesting that the slow relaxation is not an artifact of this cleaning step or the remaining residue from device fabrication steps.

Interestingly, the slow relaxation after switching the polarization UP is always significant, whereas switching the

DOI: 10.1021/acs.jpcc.7b00753
J. Phys. Chem. C 2017, 121, 7542−7548

polarization DOWN leads to a wide range of behavior from no change to convergence with the UP polarization case. One possible explanation is that the conduction state before any polarization switching events is the stable state for the UP polarization. The substrate was initially poled UP, and the surface was completely compensated before graphene transfer (Figure S2). Hence, it is possible that when the polarization is switched UP, the relaxation involves only extrinsic factors such as rearrangement of adsorbed molecules, whereas relaxation from switching polarization DOWN may involve an additional and larger energy barrier process of reversing the ferroelectric polarization direction. It has been shown that a ferroelectric thin film with an uncompensated surface can lead to domain wall formation and promotion of back-switching into a polydomain state to minimize depolarization effects.[37] Then, a varying degree of polydomain states, especially for the DOWN polarization case where it may be more likely to result in an uncompensated surface, can lead to a varying degree of slow relaxation. Alternatively, the range of behavior may be entirely due to dynamic screening processes arising from equilibration of charged or polar adsorbates, which can be sensitive to variations in the surroundings as well as to the history of the sample. Whether the long time-scale relaxation and its varying degree from device to device arise from an adsorbate-induced screening process, actual changes in the ferroelectric polarization orientation, or a combination thereof remains unclear and are mere speculation without direct experimental evidence. In this regard, PFM imaging of the polarization domain landscape underneath the graphene channel to correlate to the observed electrical response can provide much needed insights.

Currently, direct evidence of whether there is a complete ferroelectric polarization switching under the entire graphene channel region, much less how the polarization might evolve over time, is lacking. To probe the potential role of the underlying ferroelectric domain structure directly, we performed PFM measurements through the single-layer graphene over the entire channel area of our FETs following different switching operations, as shown in Figure 3. Details of PFM measurements carried out in DART mode[40] are discussed in the Supporting Information with additional data shown in Figure S6. Specifically, we focused on devices that exhibited the extreme relaxation behavior where there is a convergence of the UP and DOWN states upon relaxation, as exemplified in Figure 2C,D. As shown in Figure 3A,C, distinct differences in the phase between UP and DOWN polarization can be seen immediately after switching. For the DOWN state, there are some small UP polarization domains that either did not fully switch or quickly relaxed after removing the switching voltage. The UP state appears to be more uniform. Some of the UP domains observed in the DOWN switched case may possibly be due to varying interfacial conditions across the channel that may locally increase the coercive voltage in these regions or cause domain growth to become pinned.

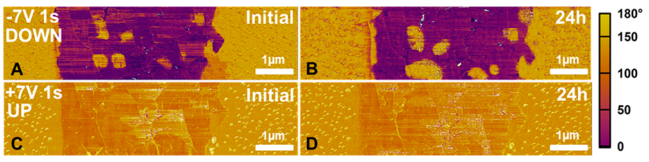

Figure 3. (A) PFM phase image of a graphene channel region following a −7 V, 1 s pulse to switch the polarization of the underlying PZT DOWN. (B) Phase image of the same channel 24 h following the initial scan indicating that the polarization remains essentially unchanged. Panels C and D are the same as panels A and B, respectively, but after a +7 V, 1 s pulse to switch the polarization of the underlying PZT UP.

What is striking from the PFM images is that 24 h after polarization switching, there is no significant change to the ferroelectric polarization domain landscape as revealed by panels B and D in Figure 3 for the DOWN and UP states, respectively. The unswitched regions in the DOWN case do grow slightly, but this small change is unlikely to account for the conductance relaxation of both UP and DOWN cases to end up with the same carrier density. Furthermore, for the UP polarization case (Figure 3C,D), there is no discernible difference between PFM images taken immediately and 24 h after the polarization switching; however, there is still a large conductance relaxation. Hence, extrinsic factors (charges or molecules at the interface between graphene and PZT and/or the interaction with the surrounding atmosphere) dominate the observed slow conductance relaxation.

Although we have chosen ±7 V, 1 s pulses based on PFM results to ensure complete (or at least maximum) switching of the ferroelectric polarization, the magnitude of this V_g pulse is well above the expected coercive voltage of ∼2−3 V observed in switching by sweeping V_g for our device geometry. Then, whether or not the slow conductance relaxation is an artifact of the large applied potential needs to be considered carefully. To this end, we have examined a range of pulse widths and amplitudes, as shown in Figure 4A. The difference between I_f and I_o are plotted as a function of pulse width and height. Before each switching V_g pulse, the device was reset with a corresponding positive or negative 7 V, 1 s pulse and allowed to relax over 250 s to ensure that the initial state was oppositely poled. Similar results were seen without this reset pulse with the exception of overlapping data points in the low-voltage regime where no apparent switching of the ferroelectric polarization occurs. Pulse amplitude of −3 V does not appear

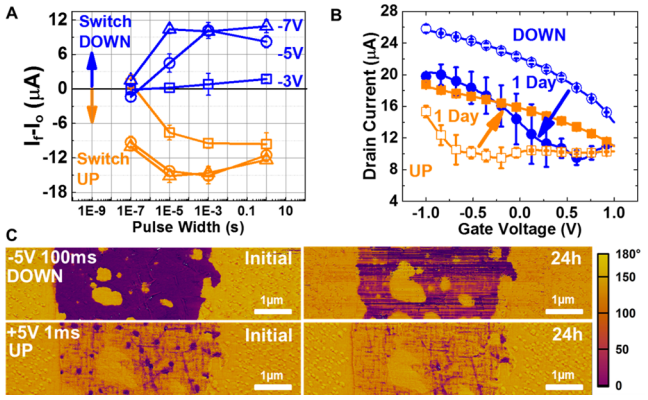

Figure 4. (A) Drain current 250 s after the switching pulse was applied for several different pulse widths and heights. The errors for the *y*-axis were estimated using the same method discussed in Figure 2E. (B) Transfer curves ∼250 s and 24 h after switching polarization of the PZT gate oxide. The errors were estimated using the same method discussed in Figure 1C. (C) Corresponding PFM phase images again showing that, even under these milder switching conditions, electrical conductance relaxation occurs without the corresponding polarization change.

DOI: 10.1021/acs.jpcc.7b00753
J. Phys. Chem. C 2017, 121, 7542−7548

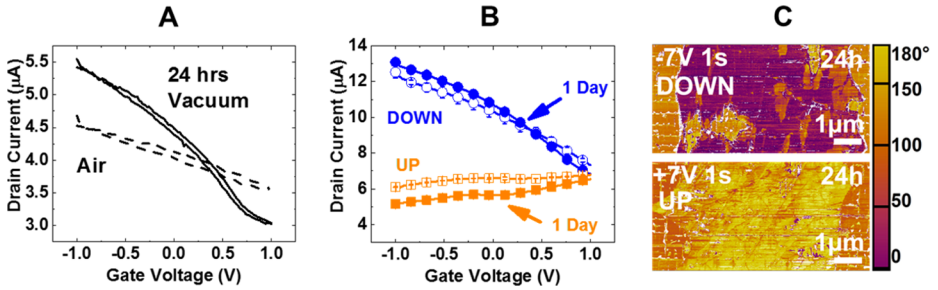

Figure 5. (A) I_d−V_g characteristics of a graphene-PZT FET measured in air and 24 h after placing in vacuum. (B) I_d−V_g characteristics in vacuum after the same switching experiments as in air as shown in Figure 2. The error bars were estimated using the same method discussed in Figure 1C. (C) PFM phase images of a device that was switched in vacuum confirming polarization switch.

to cause sufficient change in the conductance of graphene (and therefore presumably the polarization direction of the underlying PZT) even at 1 s pulse width. With +3 V pulse, 1 s appears to be the minimum duration needed to cause conductance change in graphene consistent with full polarization switch. For 5 V pulse magnitude, the minimum pulse widths needed appears to be ∼10 μs and ∼1 ms to achieve magnitude of change in conductance consistent with fully switching the polarization UP and DOWN, respectively.

Using conditions close to the above minimum V_g pulse magnitude and duration requirement, slow conductance relaxation was examined by electrical and PFM measurements. Figure 4B,C shows that using −5 V, 100 ms and +5 V, 1 ms V_g pulses leads to a response that is essentially identical to that of the ±7 V, 1 s V_g pulse cases. That is, the same conductance relaxation within 24 h of switching occurs without the corresponding changes in the actual polarization of the PZT. The relaxation observed in the DOWN state shows a small growth of the UP domains similar to the relaxation behavior observed in the −7 V, 1 s case discussed above. In the case of switching the polarization UP with +5 V, 1 ms pulse, initial PFM shows many small ∼200 nm diameter circular DOWN polarized domains, indicating that this combination of amplitude and duration of V_g pulse is actually slightly insufficient to cause complete switching. However, there is already a maximum change electrically under these conditions. The small DOWN polarized domains disappear over 24 h, leading to a more homogeneously UP poled PZT. One would then expect the graphene to slowly become more n-type, completely opposite to the observed shifting to p-type. Hence, we conclude that the slow conductance relaxation is not an artifact of the large V_g pulse amplitude and that it occurs while the polarization of the underlying PZT remains essentially unaltered.

Because the observed slow conductance relaxation is not correlated to the underlying polarization of the PZT, its origin must arise from graphene interacting with the ambient surrounding and/or with the interfacial states and molecules in between graphene and PZT. Indeed, a previous report has suggested that H_2O and its dissociated ions at the interface between a few-layer graphene and PZT can cause a slow conductance relaxation.[18] The substrate was also maintained at room temperature throughout to minimize altering the graphene−ferroelectric interface. Figure 5A shows how V_g dependence of I_d evolves after placing the devices in vacuum. Graphene becomes less p-type, presumably due to the removal of adsorbed molecules. After allowing the devices to equilibrate in vacuum for 24 h, ferroelectric polarization switching via ±7 V, 1 s pulses was repeated as in the air ambient conditions. Figure 5B shows I_d−V_g characteristics measured 250 s and 24 h after switching for both the UP and DOWN polarization states. The conductance relaxation over the course of a day appears to be significantly suppressed for both cases. There is, however, some relaxation over a longer time period of ∼1 week, as shown in Figure S7. Nevertheless, it is clear that placing graphene−PZT FETs in vacuum strongly reduces the relaxation process, similar to a previous report of long-term retention in vacuum.[19] We note that for a few-layer mechanically exfoliated graphene on PZT, essentially a complete conductance relaxation was seen within a few hours under vacuum, but there may be a different dominating mechanism in this case due to differently prepared materials and fabrication steps.[18] Because it is unlikely that placing the devices in vacuum at room temperature changes the interface between graphene and PZT significantly, the slow conductance relaxation observed in our case is likely to arise from interactions with ambient molecules in air. Once the sample was removed from vacuum and placed in air, the slow conductance relaxation returned. PFM images taken in air following polarization switching in vacuum show that the polarization had indeed switched and remain switched while in vacuum (Figure 5C). These observations point to the equilibration of adsorbates on graphene upon polarization switching of the underlying ferroelectric gate dielectric to be the origin of the slow conductance relaxation.

The above observations suggest that the switching of the underlying ferroelectric polarization leads to Fermi level position change in graphene that (partially) compensates the polarization change initially, but the subsequent interaction with the surrounding environment leads to charge transfer and changes in screening by adsorbates on the graphene. This equilibration with the ambient surroundings in turn causes the observed conductance relaxation. When this equilibration occurs, the polarization of the ferroelectric remains essentially unchanged. Then the interactions with the ambient adsorbates must also compensate the ferroelectric polarization that graphene used to. It should be noted that a slow relaxation was not observed for graphene FETs with a ferroelectric top gate dielectric, but the thick 200 nm ferroelectric polymer film may be isolating graphene from the ambient atmosphere.[34] Additionally, a significantly smaller remnant polarization of ferroelectric polymers may lead to less of a magnitude and driving force for relaxation induced by adsorbates. The combined effects of exposure to the surrounding environment and high polarization fields may make our devices more susceptible to a range of charge compensation mechanisms.

Previously proposed mechanisms that can affect polarization compensation include O-derived defects on graphene interact-

DOI: 10.1021/acs.jpcc.7b00753
J. Phys. Chem. C 2017, 121, 7542−7548

ing with the substrate surface,[26] dynamic dissociation−recombination of H_2O chemisorbed on ferroelectric surface,[18] dipole orientation of trapped H_2O molecules,[24] and trapped surface charges.[25] However, all of these mechanisms involve effects arising at the interface between graphene and the ferroelectric oxide and therefore are not likely to account for the differences in air versus under vacuum conditions observed here and the polarization of the underlying substrate remaining unchanged through the slow conductance relaxation. Following Levesque et al., we then consider the H_2O/O_2 redox process on the surface of graphene facilitated by the polar substrate surface similar to what has been considered for graphene FETs on SiO_2:[41]

$$O_2(aq) + 4H^+ + 4e^-(\text{graphene}) \rightleftharpoons 2H_2O \quad (1)$$

Equilibration with the H_2O/O_2 redox couple results in charge transfer to and from the graphene depending on the initial Fermi level position of the graphene. When the ferroelectric polarization of the underlying substrate is switched, it causes a change in carrier density in graphene. This change in turn drives adsorption of H_2O and O_2 molecules from the surroundings which will then lead to charge transfer to and from graphene through the redox reaction 1. The time scale of this process is several hours,[41] consistent with the slow kinetics we observe. Polar molecules and/or charged species can also contribute to compensating the ferroelectric polarization, resulting in stable ferroelectric domain landscape. We note that this redox reaction could, at least in part, account for the observed change in carrier density in graphene being smaller than that needed to fully compensate polarization switch in the ferroelectric oxide. Under vacuum conditions, there is less H_2O and O_2 available from the atmosphere, changing the equilibrium state and therefore causing larger Fermi level shift in graphene upon polarization switching and eliminating or reducing slow conductance relaxation.

CONCLUSIONS

We have shown that there is a conductance relaxation process that occurs over several hours after polarization switching in graphene FETs utilizing PZT as the ferroelectric gate oxide. The magnitude of the conductance relaxation varies from device to device, but there is consistently a significant relaxation upon switching the polarization UP, whereas the relaxation upon switching DOWN can vary from essentially no change to complete change that leads to the convergence of the two polarization-induced conduction states into what appears to be the same state. Direct PFM imaging of the polarization domain landscape underneath the entire graphene channel has revealed that the polarization of the underlying PZT remains essentially unchanged during this electrical relaxation process. Measurements carried out in vacuum indicate that the slow conductance relaxation is associated with equilibration with adsorbates from the ambient surroundings. We suggest the H_2O/O_2 redox couple that has been shown to exhibit similar slow equilibration with graphene on Si/SiO_2 substrate as a possible origin of the conductance relaxation upon ferroelectric polarization switching.

ASSOCIATED CONTENT

Supporting Information

The Supporting Information is available free of charge on the ACS Publications website at DOI: 10.1021/acs.jpcc.7b00753.

Extended description of PFM measurements; Raman spectrum of graphene used in this study (Figure S1); PFM data of the substrate before device fabrication and after tip bias-induced polarization switching (Figure S2); AFM images and electrical data before and after cleaning graphene with an AFM tip (Figure S3); drain and gate current dependence on gate voltage upon sweeping above the coercive voltage (Figure S4); electrical data demonstrating calculation of current change upon switching and relaxation (Figure S5); representative extended data obtained by DART-PFM measurements (Figure S6); evolution of gate dependence in vacuum over the course of a week (Figure S7) (PDF)

AUTHOR INFORMATION

Corresponding Author

*E-mail: mshim@illinois.edu.

ORCID

Steven P. Rogers: 0000-0003-1554-4142

Moonsub Shim: 0000-0001-7781-1029

Notes

The authors declare no competing financial interest.

ACKNOWLEDGMENTS

This material is based upon work supported in part by the National Science Foundation and the Nanoelectronics Research Initiative under Grant DMR-1124696. R.X. acknowledges support from the National Science Foundation under Grant DMR-1451219. S.P. acknowledges support from the National Science Foundation under Grant CMMI-1434147. L.W.M. acknowledges support from the National Science Foundation under Grant DMR-1608938. Experiments were partially carried out in the Materials Research Laboratory Central Facilities, University of Illinois.

REFERENCES

(1) Novoselov, K. S.; Geim, A. K.; Morozov, S. V.; Jiang, D.; Katsnelson, M. I.; Grigorieva, I. V.; Dubonos, S. V.; Firsov, A. A. Two-Dimensional Gas of Massless Dirac Fermions in Graphene. *Nature* **2005**, *438*, 197−200.

(2) Geim, A. K.; Novoselov, K. S. The Rise of Graphene. *Nat. Mater.* **2007**, *6*, 183−191.

(3) Kim, K. S.; Zhao, Y.; Jang, H.; Lee, S. Y.; Kim, J. M.; Kim, K. S.; Ahn, J.-H.; Kim, P.; Choi, J.-Y.; Hong, B. H. Large-Scale Pattern Growth of Graphene Films for Stretchable Transparent Electrodes. *Nature* **2009**, *457*, 706−710.

(4) Li, X.; Cai, W.; An, J.; Kim, S.; Nah, J.; Yang, D.; Piner, R.; Velamakanni, A.; Jung, I.; Tutuc, E.; et al. Large-Area Synthesis of High-Quality and Uniform Graphene Films on Copper Foils. *Science* **2009**, *324*, 1312−1314.

(5) Zhang, Y.; Gomez, L.; Ishikawa, F. N.; Madaria, A.; Ryu, K.; Wang, C.; Badmaev, A.; Zhou, C. Comparison of Graphene Growth on Single-Crystalline and Polycrystalline Ni by Chemical Vapor Deposition. *J. Phys. Chem. Lett.* **2010**, *1*, 3101−3107.

(6) Schedin, F.; Geim, A. K.; Morozov, S. V.; Hill, E. W.; Blake, P.; Katsnelson, M. I.; Novoselov, K. S. Detection of Individual Gas Molecules Adsorbed on Graphene. *Nat. Mater.* **2007**, *6*, 652−655.

(7) Wehling, T. O.; Novoselov, K. S.; Morozov, S. V.; Vdovin, E. E.; Katsnelson, M. I.; Geim, A. K.; Lichtenstein, A. I. Molecular Doping of Graphene. *Nano Lett.* **2008**, *8*, 173−177.

(8) Abbas, A. N.; Liu, G.; Liu, B.; Zhang, L.; Liu, H.; Ohlberg, D.; Wu, W.; Zhou, C. Patterning, Characterization, and Chemical Sensing Applications of Graphene Nanoribbon Arrays Down to 5 nm Using Helium Ion Beam Lithography. *ACS Nano* **2014**, *8*, 1538−1546.

(9) Yin, P. T.; Kim, T.-H.; Choi, J.-W.; Lee, K.-B.; Wan, M. M.; Yang, B. W.; Chang, G. H.; Sun, X. P.; Liu, Z. F.; Haick, H.; et al. Prospects for Graphene-Nanoparticle-Based Hybrid Sensors. *Phys. Chem. Chem. Phys.* **2013**, *15*, 12785−12799.
(10) Bae, S.; Kim, H.; Lee, Y.; Xu, X.; Park, J.-S.; Zheng, Y.; Balakrishnan, J.; Lei, T.; Ri Kim, H.; Song, Y.; et al. Roll-to-Roll Production of 30-Inch Graphene Films for Transparent Electrodes. *Nat. Nanotechnol.* **2010**, *5*, 574−578.
(11) Polat, E. O.; Uzlu, H. B.; Balci, O.; Kakenov, N.; Kovalska, E.; Kocabas, C. Graphene-Enabled Optoelectronics on Paper. *ACS Photonics* **2016**, *3*, 964−971.
(12) Reddy, D.; Register, L. F.; Carpenter, G. D.; Banerjee, S. K. Graphene Field-Effect Transistors. *J. Phys. D: Appl. Phys.* **2011**, *44*, 313001.
(13) Meric, I.; Han, M. Y.; Young, A. F.; Ozyilmaz, B.; Kim, P.; Shepard, K. L. Current Saturation in Zero-Bandgap, Top-Gated Graphene Field-Effect Transistors. *Nat. Nanotechnol.* **2008**, *3*, 654−659.
(14) Yun, J.; Lee, G.; Kim, K. S. Electron Transport in Graphene Nanoribbon Field-Effect Transistor under Bias and Gate Voltages: Isochemical Potential Approach. *J. Phys. Chem. Lett.* **2016**, *7*, 2478−2482.
(15) Wang, X.; Xie, W.; Xu, J.-B. Graphene Based Non-Volatile Memory Devices. *Adv. Mater.* **2014**, *26*, 5496−5503.
(16) Hong, X.; Posadas, A.; Zou, K.; Ahn, C.; Zhu, J. High-Mobility Few-Layer Graphene Field Effect Transistors Fabricated on Epitaxial Ferroelectric Gate Oxides. *Phys. Rev. Lett.* **2009**, *102*, 136808.
(17) Kim, Y.; Bae, C.; Ryu, K.; Ko, H.; Kim, Y. K.; Hong, S.; Shin, H. Origin of Surface Potential Change during Ferroelectric Switching in Epitaxial $PbTiO_3$ Thin Films Studied by Scanning Force Microscopy. *Appl. Phys. Lett.* **2009**, *94*, 032907.
(18) Hong, X.; Hoffman, J.; Posadas, A.; Zou, K.; Ahn, C. H.; Zhu, J. Unusual Resistance Hysteresis in n-Layer Graphene Field Effect Transistors Fabricated on Ferroelectric Pb $(Zr_{0.2}Ti_{0.8})$ O_3. *Appl. Phys. Lett.* **2010**, *97*, 033114.
(19) Song, E. B.; Lian, B.; Kim, S. M.; Lee, S.; Chung, T.-K.; Wang, M.; Zeng, C.; Xu, G.; Wong, K.; Zhou, Y. Robust Bi-Stable Memory Operation in Single-Layer Graphene Ferroelectric Memory. *Appl. Phys. Lett.* **2011**, *99*, 042109.
(20) Zheng, Y.; Ni, G.-X.; Bae, S.; Cong, C.-X.; Kahya, O.; Toh, C.-T.; Kim, H. R.; Im, D.; Yu, T.; Ahn, J. H.; et al. Wafer-Scale Graphene/Ferroelectric Hybrid Devices for Low-Voltage Electronics. *Europhys. Lett.* **2011**, *93*, 17002.
(21) Hong, X.; Zou, K.; DaSilva, A. M.; Ahn, C. H.; Zhu, J. Integrating Functional Oxides with Graphene. *Solid State Commun.* **2012**, *152*, 1365−1374.
(22) Baeumer, C.; Rogers, S. P.; Xu, R.; Martin, L. W.; Shim, M. Tunable Carrier Type and Density in Graphene/$PbZr_{0.2}Ti_{0.8}O_3$ Hybrid Structures through Ferroelectric Switching. *Nano Lett.* **2013**, *13*, 1693−1698.
(23) Rajapitamahuni, A.; Hoffman, J.; Ahn, C. H.; Hong, X. Examining Graphene Field Effect Sensors for Ferroelectric Thin Film Studies. *Nano Lett.* **2013**, *13*, 4374−4379.
(24) Lu, H.; Lipatov, A.; Ryu, S.; Kim, D. J.; Lee, H.; Zhuravlev, M. Y.; Eom, C. B.; Tsymbal, E. Y.; Sinitskii, A.; Gruverman, A. Ferroelectric Tunnel Junctions with Graphene Electrodes. *Nat. Commun.* **2014**, *5*, 5518.
(25) Yusuf, M. H.; Nielsen, B.; Dawber, M.; Du, X. Extrinsic and Intrinsic Charge Trapping at the Graphene/Ferroelectric Interface. *Nano Lett.* **2014**, *14*, 5437−5444.
(26) Baeumer, C.; Saldana-Greco, D.; Martirez, J. M. P.; Rappe, A. M.; Shim, M.; Martin, L. W. Ferroelectrically Driven Spatial Carrier Density Modulation in Graphene. *Nat. Commun.* **2015**, *6*, 6136.
(27) Ma, C.; Gong, Y.; Lu, R.; Brown, E.; Ma, B.; Li, J.; Wu, J. Detangling Extrinsic and Intrinsic Hysteresis for Detecting Dynamic Switch of Electric Dipoles Using Graphene Field-Effect Transistors on Ferroelectric Gates. *Nanoscale* **2015**, *7*, 18489−18497.
(28) Park, N.; Kang, H.; Park, J.; Lee, Y.; Yun, Y.; Lee, J.-H.; Lee, S.-G.; Lee, Y. H.; Suh, D. Ferroelectric Single-Crystal Gated Graphene/Hexagonal-BN/Ferroelectric Field-Effect Transistor. *ACS Nano* **2015**, *9*, 10729−10736.
(29) Hinnefeld, J. H.; Xu, R.; Rogers, S.; Pandya, S.; Shim, M.; Martin, L. W.; Mason, N. Single Gate p-n Junctions in Graphene-Ferroelectric Devices. *Appl. Phys. Lett.* **2016**, *108*, 203109.
(30) Hsieh, C.-Y.; Chen, Y.-T.; Tan, W.-J.; Chen, Y.-F.; Shih, W. Y.; Shih, W.-H. Graphene-Lead Zirconate Titanate Optothermal Field Effect Transistors. *Appl. Phys. Lett.* **2012**, *100*, 113507.
(31) Ni, G.-X.; Zheng, Y.; Bae, S.; Tan, C. Y.; Kahya, O.; Wu, J.; Hong, B. H.; Yao, K.; Özyilmaz, B. Graphene-Ferroelectric Hybrid Structure for Flexible Transparent Electrodes. *ACS Nano* **2012**, *6*, 3935−3942.
(32) Zheng, Y.; Ni, G.-X.; Toh, C.-T.; Tan, C.-Y.; Yao, K.; Özyilmaz, B. Graphene Field-Effect Transistors with Ferroelectric Gating. *Phys. Rev. Lett.* **2010**, *105*, 166602.
(33) Zheng, Y.; Ni, G.-X.; Toh, C.-T.; Zeng, M.-G.; Chen, S.-T.; Yao, K.; Özyilmaz, B. Gate-Controlled Nonvolatile Graphene-Ferroelectric Memory. *Appl. Phys. Lett.* **2009**, *94*, 163505.
(34) Raghavan, S.; Stolichnov, I.; Setter, N.; Heron, J.-S.; Tosun, M.; Kis, A. Long-Term Retention in Organic Ferroelectric-Graphene Memories. *Appl. Phys. Lett.* **2012**, *100*, 023507.
(35) Jie, W.; Hui, Y. Y.; Chan, N. Y.; Zhang, Y.; Lau, S. P.; Hao, J. Ferroelectric Polarization Effects on the Transport Properties of Graphene/PMN-PT Field Effect Transistors. *J. Phys. Chem. C* **2013**, *117*, 13747−13752.
(36) Lines, M. E.; Glass, A. M. *Principles and Applications of Ferroelectrics and Related Materials*; Oxford University Press: New York, 2001.
(37) Lichtensteiger, C.; Fernandez-Pena, S.; Weymann, C.; Zubko, P.; Triscone, J.-M. Tuning of the Depolarization Field and Nanodomain Structure in Ferroelectric Thin Films. *Nano Lett.* **2014**, *14*, 4205−4211.
(38) Paruch, P.; Posadas, A.-B.; Dawber, M.; Ahn, C. H.; McEuen, P. L. Polarization Switching Using Single-Walled Carbon Nanotubes Grown on Epitaxial Ferroelectric Thin Films. *Appl. Phys. Lett.* **2008**, *93*, 132901.
(39) Huang, P. Y.; Ruiz-Vargas, C. S.; van der Zande, A. M.; Whitney, W. S.; Levendorf, M. P.; Kevek, J. W.; Garg, S.; Alden, J. S.; Hustedt, C. J.; Zhu, Y.; et al. Grains and Grain Boundaries in Single-Layer Graphene Atomic Patchwork Quilts. *Nature* **2011**, *469*, 389−392.
(40) Rodriguez, B. J.; Callahan, C.; Kalinin, S. V.; Proksch, R. Dual-Frequency Resonance-Tracking Atomic Force Microscopy. *Nanotechnology* **2007**, *18*, 475504.
(41) Levesque, P. L.; Sabri, S. S.; Aguirre, C. M.; Guillemette, J.; Siaj, M.; Desjardins, P.; Szkopek, T.; Martel, R. Probing Charge Transfer at Surfaces Using Graphene Transistors. *Nano Lett.* **2011**, *11*, 132−137.

DOI: 10.1021/acs.jpcc.7b00753
J. Phys. Chem. C 2017, 121, 7542−7548